Iterated perturbation theory for the attractive Holstein and Hubbard models

J. K. Freericks

Department of Physics, University of California, Davis, California 95616

Mark Jarrell

Department of Physics, University of Cincinnati, Cincinnati, Ohio 45221

(Received 18 March 1994)

A strictly truncated (weak-coupling) perturbation theory is applied to the attractive Holstein and Hubbard models in infinite dimensions. These results are qualified by comparison with essentially exact quantum Monte Carlo results. The second-order iterated perturbation theory is shown to be quite accurate in calculating transition temperatures for retarded interactions, but is not as accurate for the self-energy or the irreducible vertex functions themselves. Iterated perturbation theory is carried out through fourth order for the Hubbard model. The self-energy is quite accurately reproduced by the theory, but the vertex functions are not. Anomalous behavior occurs near half-filling because the iterated perturbation theory is not a conserving approximation.

I. INTRODUCTION

Recently Metzner and Vollhardt[1] showed that the fermionic many-body problem simplifies in the limit of infinite spatial dimensions, d. The $d \to \infty$ limit is taken in such a fashion that the dynamics are local in space, and the lattice problem can be mapped onto a self-consistently embedded Anderson impurity model. The self-energy and irreducible vertex functions of the impurity problem are employed to determine the Green's functions and susceptibilities of the infinite-dimensional lattice. This many-body problem can essentially be solved exactly by using the quantum Monte Carlo (QMC) techniques of Hirsch and Fye[2] to extract the self-energy and irreducible vertex functions of the relevant impurity problem. A variety of models have already been examined in this fashion: the Hubbard model,[3-6] periodic Anderson model,[7] and the Holstein model.[8]

The infinite-dimensional limit provides a unique testing ground for various approximation techniques, since one can compare them to the benchmark QMC results. Previous work has concentrated on the strong-coupling limit[9,10] (perturbation theory in the kinetic energy) which can be shown to be an excellent approximation in the region of moderate to strong coupling.

Calculations in the weak-coupling limit are not under as good control. The main emphasis so far has been on conserving approximations[11-14] (such as the fluctuation-exchange approximation) to the many-body problem. Conserving approximations are popular because they satisfy the requisite conservation laws for electronic charge, energy, and momentum.[15] It turns out, however, that conserving approximations suffer from some serious flaws: (1) truncated approximations (through fourth order) do not show a turnover in T_c as the strong-coupling regime is approached; (2) infinite summations of certain classes of diagrams can produce a turnover in T_c, but the self-energy is overestimated, and many-body features

(such as the upper and lower Hubbard bands) do not appear in the single-particle spectral function. Similar deficiencies where found by White in his examination of the Anderson impurity model itself.[16]

An alternate approximation scheme, which does not suffer from the above problems (but is not conserving), has been introduced by Georges and Kotliar[17] and is known as iterated perturbation theory (IPT). In this case, the perturbation theory is strictly truncated at a finite order (as opposed to a conserving approximation that sums the infinite class of diagrams corresponding to self-energy insertions into the dressed Green's function). The motivation for this approximation comes from the pioneering work of Yosida and Yamada,[18] who found that truncated perturbation theory was an extremely accurate approximation for the Anderson impurity model because the sum total of all classes of diagrams at a given order is an order of magnitude smaller than any of its constituent parts. This remarkable near cancellation of diagrams was further verified to high order by Zlatić and Horvatić[19] who found that the exact Bethe ansatz solutions can be rearranged into a power series whose coefficients die off rapidly.

Horvatić and Zlatić[20] generalized Yosida and Yamada's analysis off of half-filling and found that the strictly truncated perturbation series was also accurate in the doped case. However, anomalous behavior begins to enter if the coupling strength is increased too far and the electron concentration is close to half-filling. Ferrer, Martín-Rodero, and Flores[21] realized that the reason why the perturbation theory fails more rapidly away from half-filling is because the second-order perturbation theory correctly reproduces the atomic limit at half-filling, but not away from half-filling. They proposed an *ad hoc* interpolation scheme that properly reproduces the atomic limit everywhere and removes some of the anomalous behavior of the Horvatić- Zlatić approximation. An alternate interpolation scheme has been proposed by Neal[22]

based upon functional integral techniques which appears to be quite accurate for all values of the interaction strength but is restricted to half-filling.

In this paper, we will examine the iterated perturbation theory through second order for the Holstein model and through fourth order for the negative-U Hubbard model. Comparison of the self-energy, the irreducible vertex functions, and the transition temperatures will be made to the exact QMC solutions. In Sec. II the infinite-dimensional formalism is reviewed along with the details of the IPT approximation. Sec. III contains the results for the Holstein model, while Sec. IV holds the results for the Hubbard model. Conclusions and discussion follow in Sec. V.

II. FORMALISM

The electron-phonon interaction is generally believed to be responsible for the superconductivity in most low-temperature superconductors.[23,24] The conventional theory used to describe superconductivity was introduced by Migdal[25] and Eliashberg.[26] Migdal-Eliashberg (ME) theory ignores vertex corrections which can be shown to be proportional to powers of the Debye frequency divided by the Fermi energy, and hence are small corrections for most real materials.

Here, iterated perturbation theory is examined in a systematic fashion for the attractive electron-phonon interaction described by the Holstein[27] model (the effects of Coulomb repulsion are explicitly neglected). The Holstein model consists of conduction electrons that interact with localized (Einstein) phonons:

$$H = -\frac{t^*}{2\sqrt{d}} \sum_{\langle j,k \rangle \sigma} (c_{j\sigma}^\dagger c_{k\sigma} + c_{k\sigma}^\dagger c_{j\sigma})$$
$$+ \sum_j (gx_j - \mu)(n_{j\uparrow} + n_{j\downarrow} - 1)$$
$$+ \frac{1}{2} M\Omega^2 \sum_j x_j^2 + \frac{1}{2} \sum_j \frac{p_j^2}{M} , \qquad (1)$$

where $c_{j\sigma}^\dagger$ ($c_{j\sigma}$) creates (destroys) an electron at site j with spin σ, $n_{j\sigma} = c_{j\sigma}^\dagger c_{j\sigma}$ is the electron number operator, and x_j (p_j) is the phonon coordinate (momentum) at site j. The hopping matrix elements connect the nearest neighbors of a hypercubic lattice in d dimensions. The unit of energy is chosen to be the rescaled matrix element t^*. The phonon has a mass M (chosen to be $M = 1$), a frequency Ω, and a spring constant $\kappa \equiv M\Omega^2$ associated with it. The electron-phonon coupling constant (deformation potential) is denoted by g; the effective electron-electron interaction strength is then the bipolaron binding energy

$$U \equiv -\frac{g^2}{M\Omega^2} = -\frac{g^2}{\kappa}. \qquad (2)$$

The chemical potential is denoted by μ and particle-hole symmetry occurs for $\mu = 0$.

In the instantaneous limit where U remains finite and g and Ω are large compared to the bandwidth ($g, \Omega \rightarrow$

$\infty, U =$ finite), the Holstein model maps onto the attractive Hubbard model[28]

$$H = -\frac{t^*}{2\sqrt{d}} \sum_{\langle j,k \rangle \sigma} (c_{j\sigma}^\dagger c_{k\sigma} + c_{k\sigma}^\dagger c_{j\sigma}) - \mu \sum_j (n_{j\uparrow} + n_{j\downarrow})$$
$$+ U \sum_j (n_{j\uparrow} - \tfrac{1}{2})(n_{j\downarrow} - \tfrac{1}{2}) , \qquad (3)$$

with U defined by Eq. (2).

The infinite-dimensional limit of Metzner and Vollhardt[1] is taken ($d \rightarrow \infty$), in which the electronic many-body problem becomes a local (impurity) problem that retains its complicated dynamics in time. The hopping integral is scaled to zero in such a fashion that the free-electron kinetic energy remains finite while the self-energy for the single-particle Green's function and the irreducible vertex functions have no momentum dependence and are functionals of the local Green's function.[1,29,30] This limit retains the strong-correlation effects that arise from trying to simultaneously minimize both the kinetic energy and the potential energy.

The many-body problem is solved by mapping it onto an auxiliary impurity problem[31,32] in a time-dependent field that mimics the hopping of an electron onto a site at time τ and off the site at a time τ'. The action for the impurity problem is found by integrating out the degrees of freedom associated with other lattice sites in a path-integral formalism.[17] The result is an effective action

$$S_{\text{eff}} = \sum_\sigma \int_0^\beta d\tau \int_0^\beta d\tau' c_\sigma^\dagger(\tau) G_0^{-1}(\tau - \tau') c_\sigma(\tau')$$
$$+ \sum_\sigma \int_0^\beta d\tau [gx(\tau) - \mu][c_\sigma^\dagger(\tau) c_\sigma(\tau) - \tfrac{1}{2}] ,$$
$$+ \tfrac{1}{2} M \int_0^\beta d\tau [\Omega^2 x^2(\tau) + \dot{x}^2(\tau)] \qquad (4)$$

where G_0^{-1} is the "bare" Green's function that contains *all of the dynamical information of the other sites of the lattice.* The interacting Green's function, defined to be

$$G(i\omega_n) \equiv -\int_0^\beta d\tau e^{i\omega_n \tau} \frac{\text{Tr}\langle e^{-\beta H} T_\tau c(\tau) c^\dagger(0) \rangle}{\text{Tr}\langle e^{-\beta H} \rangle} , \qquad (5)$$

is determined by Dyson's equation

$$G_n^{-1} \equiv G^{-1}(i\omega_n) = G_0^{-1}(i\omega_n) - \Sigma(i\omega_n). \qquad (6)$$

A self-consistency relation is required in order to determine the bare Green's function G_0. This is achieved by mapping the impurity problem onto the infinite-dimensional lattice thereby equating the full Green's function for the impurity problem with the local Green's function for the lattice,

$$G_{jj}(i\omega_n) = \sum_k G(\mathbf{k}, i\omega_n)$$
$$= \sum_k [i\omega_n + \mu - E(\mathbf{k}) - \Sigma(i\omega_n)]^{-1}$$
$$= F_\infty[i\omega_n + \mu - \Sigma(i\omega_n)]. \qquad (7)$$

Here $F_\infty(z)$ is the scaled complimentary error function of a complex argument,

$$
\begin{aligned}
F_\infty(z) &\equiv \frac{1}{\sqrt{\pi}} \int_{-\infty}^{\infty} dy \frac{\exp(-y^2)}{z-y} \\
&= -i\,\mathrm{sgn}[\mathrm{Im}(z)]\sqrt{\pi}e^{-z^2}\mathrm{erfc}\{-i\,\mathrm{sgn}[\mathrm{Im}(z)]z\}.
\end{aligned}
\tag{8}
$$

The dynamics of the (local) impurity problem are identical to the dynamics of the Anderson impurity model.[29,31,32,17,3] This many-body problem can either be solved exactly with the QMC algorithm of Hirsch and Fye,[2] or it can be approximately solved by employing a truncated perturbative expansion. The impurity is self-consistently embedded in the host, since it must satisfy the self-consistency relation in Eq. (7).

It is important to note that since one does not *a priori* know the bare Green's function G_0^{-1} in Eq. (4), one must iterate to determine a self-consistent solution for the Green's function of the infinite-dimensional lattice. This is achieved by calculating the self-energy as a functional of the bare Green's function G_0, and then determining the new local Green's function from the approximate self-energy and Eq. (7). The new bare Green's function is then calculated from the Dyson equation in Eq. (6). This process is iterated until convergence is

achieved [for the perturbation theory approximation the maximum variation of each $G(i\omega_n)$ is less than 1 part in 10^8 which typically takes between 5 and 30 iterations, for the QMC calculations the algorithm is iterated from 7 to 9 times]. Note that the iteration required to determine a self-consistent bare Green's function G_0 should not be confused with the the iterative techniques used to self-consistently sum all of the self-energy insertions in a self-consistent perturbation theory—*the perturbation series is always strictly truncated at a finite order here.*

The QMC algorithm proceeds by discretizing the imaginary-time interval from 0 to β into L time slices of equal width $\Delta\tau = \beta/L$ and evaluating the relevant path integrals in a grand canonical scheme. Both local moves, in which the phonon coordinate is shifted by a different amount at each time slice, and global moves, in which the phonon coordinate is shifted by a uniform amount for every time slice, are incorporated into the QMC algorithm[33]. The values of L used ranged from 20 to 160 with the largest values of $\Delta\tau$ reserved for the lowest temperatures (usually $\Delta\tau$ was fixed at 0.4). No sign problem was found at any filling.

Static two-particle properties are also easily calculated since the irreducible vertex function is local.[34] The static susceptibility for charge-density-wave (CDW) order is given by

$$
\begin{aligned}
\chi^{\mathrm{CDW}}(\mathbf{q}) &\equiv \frac{1}{2N} \sum_{\mathbf{R}_j-\mathbf{R}_k\sigma\sigma'} e^{i\mathbf{q}\cdot(\mathbf{R}_j-\mathbf{R}_k)} T \int_0^\beta d\tau \int_0^\beta d\tau' [\langle n_{j\sigma}(\tau)n_{k\sigma'}(\tau')\rangle - \langle n_{j\sigma}(\tau)\rangle\langle n_{k\sigma'}(\tau')\rangle] \\
&\equiv T \sum_{mn} \tilde{\chi}^{\mathrm{CDW}}(\mathbf{q},i\omega_m,i\omega_n) = T \sum_{mn} \tilde{\chi}_{mn}^{\mathrm{CDW}}(\mathbf{q}),
\end{aligned}
\tag{9}
$$

at each ordering wave vector $\mathbf{q}$. Dyson's equation for the two-particle Green's function becomes[3,34]

$$
\tilde{\chi}_{mn}^{\mathrm{CDW}}(\mathbf{q}) = \tilde{\chi}_m^0(\mathbf{q})\delta_{mn} - T \sum_p \tilde{\chi}_m^0(\mathbf{q})\Gamma_{mp}^{\mathrm{CDW}}\tilde{\chi}_{pn}^{\mathrm{CDW}}(\mathbf{q}),
\tag{10}
$$

with $\Gamma_{mn}^{\mathrm{CDW}}$ the (local) irreducible vertex function in the CDW channel.

The bare CDW susceptibility $\tilde{\chi}_n^0(\mathbf{q})$ in Eq. (10) is defined in terms of the *dressed* single-particle Green's function,

$$
\begin{aligned}
\tilde{\chi}_n^0(\mathbf{q}) &\equiv -\frac{1}{N} \sum_{\mathbf{k}} G_n(\mathbf{k})G_n(\mathbf{k}+\mathbf{q}) \\
&= -\frac{1}{\sqrt{\pi}} \frac{1}{\sqrt{1-X^2(\mathbf{q})}} \int_{-\infty}^{\infty} dy \frac{e^{-y^2}}{i\omega_n + \mu - \Sigma_n - y} \\
&\quad \times F_\infty\left[\frac{i\omega_n + \mu - \Sigma_n - X(\mathbf{q})y}{\sqrt{1-X^2(\mathbf{q})}}\right],
\end{aligned}
\tag{11}
$$

and all of the wave vector dependence is included in the scalar[31,11] $X(\mathbf{q}) \equiv \sum_{j=1}^d \cos q_j/d$. The mapping $\mathbf{q} \mapsto X(\mathbf{q})$ is a many-to-one mapping that determines an equivalence class of wave vectors in the Brillouin zone. "General" wave vectors are all mapped to $X = 0$ since

$\cos q_j$ can be thought of as a random number between -1 and 1 for "general" points in the Brillouin zone. Furthermore, all possible values of X ($-1 \le X \le 1$) can be labeled by a wave vector that lies on the diagonal of the first Brillouin zone extending from the zone center ($X = 1$) to the zone corner ($X = -1$). The presence of incommensurate order in the attractive Holstein model is restricted to a very narrow region of parameter space,[8,13] and so only the "antiferromagnetic" point $X = -1$ is considered for CDW order. The integral for $\tilde{\chi}_m^0(X)$ in Eq. (11) can then be performed analytically,[31] $\tilde{\chi}_n^0(X = -1) = -G_n/(i\omega_n + \mu - \Sigma_n)$. The irreducible vertex function $\Gamma_{mn}^{\mathrm{CDW}}$ is either directly calculated in a perturbative expansion (IPT) or is determined by inverting the Dyson equation in Eq. (10) (QMC).

A similar procedure is used for the singlet s-wave superconducting (SC) channel. The corresponding definitions are as follows: The static susceptibility in the superconducting channel is defined to be

$$
\begin{aligned}
\chi^{\mathrm{SC}}(\mathbf{q}) &\equiv \frac{1}{N} \sum_{\mathbf{R}_j-\mathbf{R}_k} e^{i\mathbf{q}\cdot(\mathbf{R}_j-\mathbf{R}_k)} T \\
&\quad \times \int_0^\beta d\tau \int_0^\beta d\tau' \langle c_{j\uparrow}(\tau)c_{j\downarrow}(\tau)c_{k\downarrow}^\dagger(\tau')c_{k\uparrow}^\dagger(\tau')\rangle \\
&= T \sum_{mn} \tilde{\chi}^{\mathrm{SC}}(\mathbf{q},i\omega_m,i\omega_n) = T \sum_{mn} \tilde{\chi}_{mn}^{\mathrm{SC}}(\mathbf{q}),
\end{aligned}
\tag{12}
$$

for superconducting pairs that carry momentum **q**; Dyson's equation becomes

$$\tilde{\chi}^{SC}_{mn}(\mathbf{q}) = \tilde{\chi}^{0}_{m}{}'(\mathbf{q})\delta_{mn} - T\sum_{p}\tilde{\chi}^{0}_{m}{}'(\mathbf{q})\Gamma^{SC}_{mp}\tilde{\chi}^{SC}_{pn}(\mathbf{q}), \quad (13)$$

with Γ^{SC}_{mn} the corresponding irreducible vertex function for the SC channel; the bare pair-field susceptibility becomes

$$\tilde{\chi}^{0}_{n}{}'(\mathbf{q}) \equiv \frac{1}{N}\sum_{\mathbf{k}}G_{n}(\mathbf{k})G_{-n-1}(-\mathbf{k}+\mathbf{q})$$

$$= \frac{1}{\sqrt{\pi}}\frac{1}{\sqrt{1-X^{2}(\mathbf{q})}}\int_{-\infty}^{\infty}dy\frac{e^{-y^{2}}}{i\omega_{n}+\mu-\Sigma_{n}-y}$$

$$\times F_{\infty}\left[\frac{i\omega_{-n-1}+\mu-\Sigma_{-n-1}-X(\mathbf{q})y}{\sqrt{1-X^{2}(\mathbf{q})}}\right], \quad (14)$$

with the special value $\tilde{\chi}^{0}_{n}{}'(X=1) = -\mathrm{Im}G_{n}/\mathrm{Im}(i\omega_{n}-\Sigma_{n})$ for the SC pair that carries no net momentum; and finally the irreducible vertex function is also either directly calculated in a perturbative expansion (IPT) or is determined by inverting the Dyson equation in Eq. (13) (QMC).

There are two different approximation schemes that can be used for determining the irreducible vertex functions in a perturbative expansion. The first scheme, denoted IPT, is in the spirit of Yosida and Yamada's original analysis:[18] The vertex functions are also expanded in a perturbation series that is strictly truncated at a finite order. In the second scheme, denoted IPT*, the fully dressed local Green's functions are used to calculate the irreducible vertex functions. In general, one might expect the IPT approximation to be more accurate than the IPT* approximation from the work of Yosida and

Yamada,[18] but the irreducible vertex functions were not investigated in their analysis of the Anderson impurity model, and so it is not *a priori* clear which will be a better approximation.

The transition temperature of the infinite-dimensional Holstein model is now found by calculating the temperature at which the relevant susceptibility diverges (CDW or SC). One can determine this transition temperature by finding the temperature where the scattering matrix (in the relevant channel)

$$T_{mn} \equiv -T\Gamma_{mn}\chi^{0}_{n} \quad (15)$$

has unit eigenvalue.[35] Note that the fully dressed Green's functions are always used in calculating the bare susceptibility χ^{0} because the bare susceptibility is a property of the infinite-dimensional lattice, and not the Anderson impurity problem, and we expect to find better agreement with the QMC results if we use the correct bare susceptibility.

III. HOLSTEIN MODEL

The diagrammatic expansion for the IPT is depicted in Figs. 1 and 2. The wiggly lines denote the bare phonon propagator, and the straight lines denote the bare Green's function G_{0}. Figure 1 shows the self-energy for the IPT approximation through second order. The self-energy includes, respectively, the Hartree term (which is a constant that is reabsorbed into the chemical potential), the Fock term, the second-order term that dresses the phonon propagator, the lowest-order vertex correction, and the second-order rainbow diagram (which corresponds to the self-energy insertion of the first-order Fock diagram into the first-order Fock diagram).

To be more explicit, the self-energy for the second-order IPT approximation is

$$\Sigma_{n} = -UT\sum_{r}\frac{\Omega^{2}}{\Omega^{2}+\nu^{2}_{n-r}}G_{0}(i\omega_{r})$$

$$+ U^{2}T^{2}\sum_{rs}\left[-2\frac{\Omega^{2}}{\Omega^{2}+\nu^{2}_{n-r}}+\frac{\Omega^{2}}{\Omega^{2}+\nu^{2}_{r-s}}\right]\frac{\Omega^{2}}{\Omega^{2}+\nu^{2}_{n-r}}G_{0}(i\omega_{r})G_{0}(i\omega_{s})G_{0}(i\omega_{n-r+s})$$

$$+ U^{2}T^{2}\sum_{rs}\frac{\Omega^{2}}{\Omega^{2}+\nu^{2}_{n-r}}\frac{\Omega^{2}}{\Omega^{2}+\nu^{2}_{r-s}}G^{2}_{0}(i\omega_{r})G_{0}(i\omega_{s}), \quad (16)$$

which includes the Fock diagram contribution and the three second-order contributions of Fig. 1. The bosonic Matsubara frequency ν_{l} is defined to be $\nu_{l} \equiv 2l\pi T$.

The self-consistency step involves first determining a new local Green's function G_{n} from the integral relation in Eq. (7) with the approximate self-energy of Eq. (16). Next the new bare Green's function is found from the Dyson equation in Eq. (6) using the same approximate self-energy. A new self-energy is then calculated from the new bare Green's function [using Eq. (16)], and the process is iterated. This iteration process terminates when the maximum deviation in the local Green's function is less than one part in 10^{8}.

Once the Green's functions and self-energies have been determined, the irreducible vertex functions can be calculated for the CDW or SC channels. In the CDW channel [see Fig. 2(a)] one must include both direct and exchange diagrams as well as the vertex corrections. The result is

$$\Gamma^{\mathrm{CDW}}_{mn} = 2U - 2U^2 T \sum_r [G_0(i\omega_r)G_0(i\omega_{m-n+r}) + G_0(i\omega_r)G_0(i\omega_{m+n-r})] \left[\frac{\Omega^2}{\Omega^2 + \nu^2_{n-r}}\right]^2$$

$$- U\frac{\Omega^2}{\Omega^2 + \nu^2_{m-n}} - 2U^2 T \sum_r G_0(i\omega_r)G_0(i\omega_{m-n+r})\frac{\Omega^2}{\Omega^2 + \nu^2_{m-n}} \left[\frac{\Omega^2}{\Omega^2 + \nu^2_{m-n}} - \frac{\Omega^2}{\Omega^2 + \nu^2_{n-r}}\right]$$

$$+ U^2 T \sum_r G_0(i\omega_r)G_0(i\omega_{m+n-r})\frac{\Omega^2}{\Omega^2 + \nu^2_{m-r}}\frac{\Omega^2}{\Omega^2 + \nu^2_{n-r}}, \qquad (17)$$

for the IPT approximation. The IPT* approximation has the same functional form as in Eq. (17), but the bare Green's function G_0 is replaced by the dressed Green's function G (this functional form is the same as the one used for the conserving approximation[14]). Note that the vertex corrections (arising from the first-order exchange diagrams) modify the *interaction* in the CDW channel so that it properly interpolates between the zero-frequency limit $\Gamma^{\mathrm{CDW}} \to 2U$ and the infinite-frequency limit $\Gamma^{\mathrm{CDW}} \to U$. At an intermediate frequency, the CDW interaction strength has a complicated temperature dependence. In the SC channel [see Fig. 2(b)] one finds

$$\Gamma^{\mathrm{SC}}_{mn} = U\frac{\Omega^2}{\Omega^2 + \nu^2_{m-n}} + U^2 T \sum_r G_0(i\omega_r)G_0(i\omega_{m-n+r})\frac{\Omega^2}{\Omega^2 + \nu^2_{m-n}} \left[2\frac{\Omega^2}{\Omega^2 + \nu^2_{m-n}} - \frac{\Omega^2}{\Omega^2 + \nu^2_{n-r}} - \frac{\Omega^2}{\Omega^2 + \nu^2_{m+r+1}}\right]$$

$$- U^2 T \sum_r G_0(i\omega_r)G_0(i\omega_{m+n+r+1})\frac{\Omega^2}{\Omega^2 + \nu^2_{m+r+1}}\frac{\Omega^2}{\Omega^2 + \nu^2_{n+r+1}}, \qquad (18)$$

for the IPT approximation. Once again, the IPT* approximation has the same functional form as in Eq. (18), but the bare Green's function G_0 is replaced by the dressed Green's function G.

At half-filling the Holstein model interaction is particle-hole symmetric, and so the Green's function and self-energy are purely imaginary and the vertices are real. The self-energy can be expressed by $\Sigma(i\omega_n) \equiv i\omega_n[1 - Z(i\omega_n)]$, with $Z(i\omega_n)$ the renormalization function for the self-energy. At half-filling, both $\chi^0_m(X = -1)$ and the maximal eigenvector of the scattering matrix are also even functions of Matsubara frequency, and so the only contribution of the irreducible vertex function to the eigenvalue of the scattering matrix comes from the even Matsubara frequency component $[\Gamma_{m,n} + \Gamma_{-m-1,n}]/2$. The same result holds for the SC channel at all fillings, because both the maximal eigenvector and the bare susceptibility are symmetric functions of Matsubara frequency.

A comparison of these approximations to the exact QMC results for the electronic self-energy and one col-

umn of the irreducible vertex function in the CDW and SC channels is made in Figs. 3–5 for three different interaction strengths at half-filling. The phonon frequency is set to be approximately one-eighth of the effective bandwidth ($\Omega/t^* = 0.5$) as was done in the QMC solutions.[8] The energy cutoff is set to include 256 positive Matsubara frequencies for the perturbative approximations.

At weak coupling ($g = 0.4$, $T = 0.0625$, Fig. 3), the second-order IPT approximation is a reasonable approximation to the electron self-energy [Fig. 3(a)] and to the CDW irreducible vertex function [Figure 3(b)]. Note that the IPT underestimates the self-energy (an effect that raises T_c) and overestimates the magnitude of the vertex (an effect that also raises T_c), and so one expects it to overestimate the CDW transition temperature (both the

FIG. 1. Dyson equation for the self-energy of the Holstein model. The solid lines denote the *bare* (electronic) Green's function G_0 and the wavy lines denote the phonon propagator. The self-energy includes the Hartree and Fock contributions, the second-order dressing of the phonon line, the lowest-order vertex correction, and the second-order rainbow diagram (which arises from the self-energy insertion of the Fock diagram into the Fock diagram).
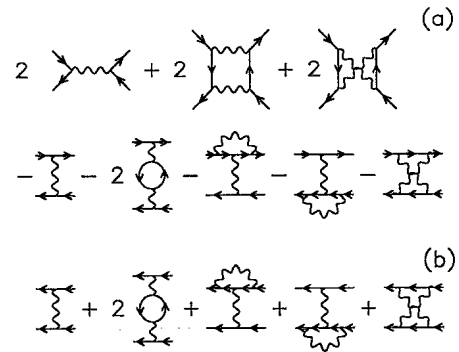

FIG. 2. The irreducible vertex functions in the CDW and SC channels. The CDW irreducible vertex function is shown in (a). Note that the vertex corrections (exchange diagrams) modify the interaction *to lowest order* in the CDW channel. The SC irreducible vertex function is shown in (b). The vertex corrections first enter at second order in the SC channel. In the IPT approximation the electron propagator is the bare Green's function G_0, while in the IPT* approximation the electron propagator is the dressed Green's function G.

IPT and the IPT* approximations yield similar results for the irreducible vertex function). Clearly third-order diagrams play an important role even at this weak a value of the coupling strength. In this sense, the IPT is less accurate for retarded interactions than it is for instantaneous interactions (see Sec. IV).

As the coupling strength is increased to the point where a double-well structure begins to develop in the effective phonon potential of the QMC simulations of Ref. 8 ($g = 0.5$, $T = 0.111$) one can see strong-coupling

effects begin to enter into the QMC vertex. The IPT still underestimates the self-energy [Fig. 4(a)], but as the strong-coupling regime is approached, the vertices become increasingly attractive [Fig. 4(b)]. This enhanced attraction is not represented by either the IPT or the IPT* approximations. Note that in this regime the self-energy and the vertices are underestimated, which implies that the transition temperature may be determined more accurately than expected, because these effects tend to cancel each other out in determining T_c. The under-
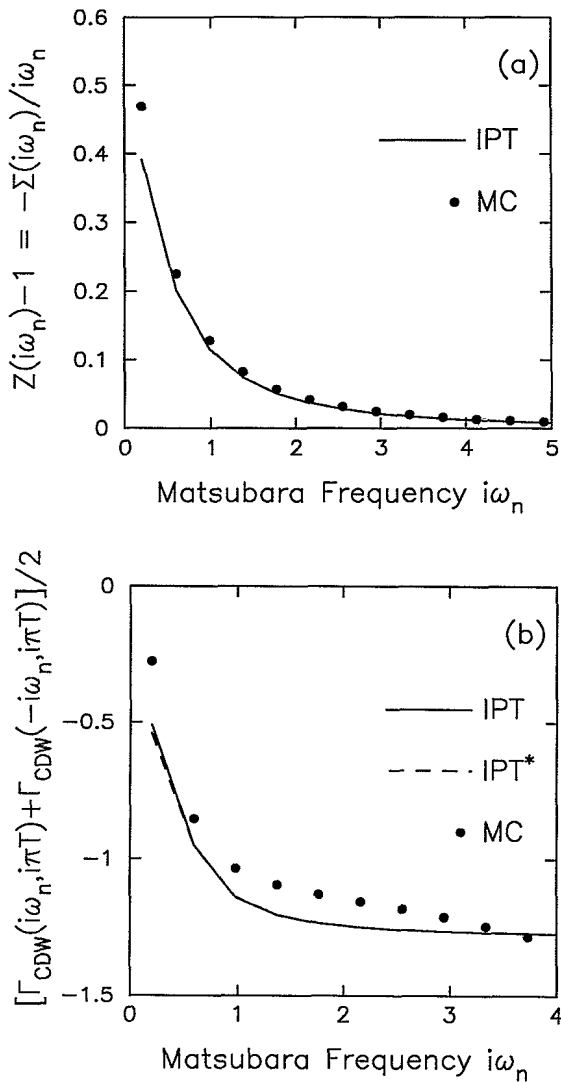

FIG. 3. Comparison of the second-order IPT (solid line) and IPT* (dashed line) to the QMC solutions (solid dots) for the Holstein model at half-filling with phonon frequency $\Omega = 0.5t^*$, interaction strength $g = 0.4t^*$, and temperature $T = t^*/16$. This example is generic for the weak-coupling limit. In (a) the self-energy renormalization function $Z(i\omega_n) - 1$ is plotted against the Matsubara frequency. In (b) the symmetric combination of the first column of the irreducible vertex function in the CDW channel is shown. Note that even at this weak a value of coupling strength the third-order diagrams must play an important role.
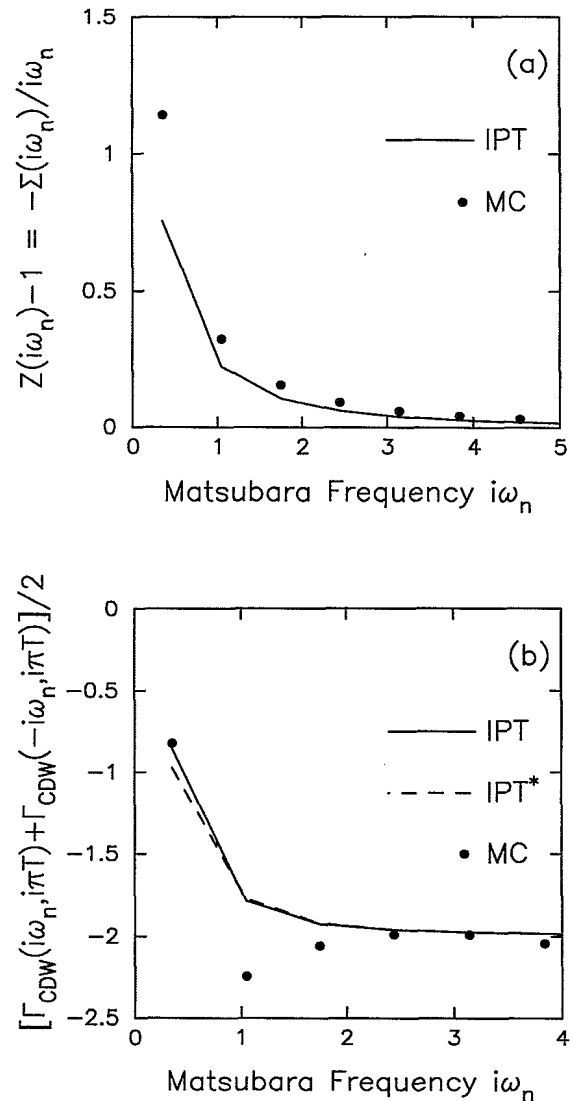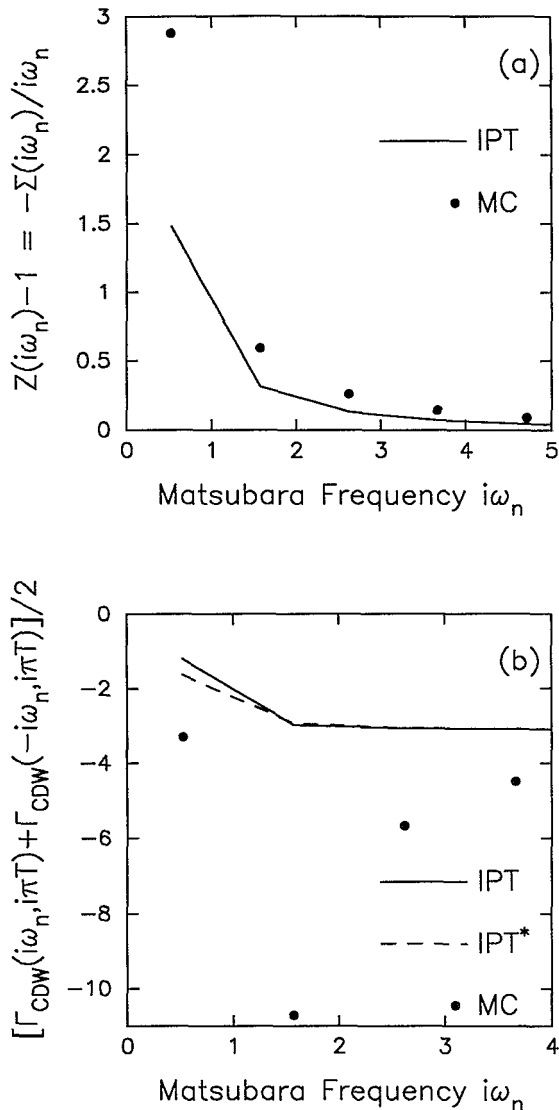
FIG. 4. Comparison of the second-order IPT (solid line) and IPT* (dashed line) to the QMC solutions (solid dots) for the Holstein model at half-filling with phonon frequency $\Omega = 0.5t^*$, interaction strength $g = 0.5t^*$, and temperature $T = t^*/9$. This example is generic for the transition region to the strong-coupling limit. The self-energy renormalization function (a) and the irreducible vertex function in the CDW channel (b) are pictured. Note that in the limit where the strong-coupling effects begin to manifest themselves, the QMC vertex becomes increasingly attractive at low-frequency transfer.

estimation of the magnitude of the vertex will eventually cause T_c to drop due to the large self-energy renormalization.

When one is well into the strong-coupling regime ($g = 0.625$, $T = 0.167$, Fig. 5) the deficiencies of the IPT approximation become more apparent. The self-energy is underestimated by almost a factor of 2 [Fig. 5(a)], and the vertices are underestimated by almost a factor of 3 at intermediate frequencies [Fig. 5(b)]. Even at this large a value of the coupling, both the IPT and IPT* approximations remain similar to each other. At this point one would say the approximate theory is failing to faithfully

represent the exact solution.

A comparison of the IPT approximation to either a second-order conserving approximation or to ME theory[14] shows that the IPT is a superior approximation for both the self-energy and the vertices, but none of these approximate methods is accurate over a wide range of interaction strength, indicating once again the importance of the third-order diagrams.

At half-filling, the Holstein model always has a transition to a CDW-ordered phase at $\mathbf{q} = (\pi, \pi, \pi, \ldots)$ ($X = -1$). The transition temperature to this commensurate CDW is plotted in Fig. 6 as a function of the interaction strength. Both second-order IPT approximations are compared to the QMC simulations.[8] The IPT and the IPT* approximations are very accurate in determining T_c; the peak position and height are both reproduced well. This result is definitely a numerical coincidence, since the self-energy and vertices are poorly approximated at the peak of the curve ($g = 0.625$). Furthermore, it is the self-energy renormalization that ultimately causes T_c to turn over, but T_c drops far too rapidly in this strong-coupling regime. This result is similar to what was found for a strong-coupling approximation:[9] There the transition temperature dropped too rapidly in the weak-coupling regime.

The IPT and IPT* approximations are superior to either a second-order conserving approximation or to ME theory in both a qualitative and a quantitative determination of the CDW transition temperature at half-filling. They also have the correct limiting behavior as $U \to 0$ because they are second-order perturbation theories.[36,37,14]

As the system is doped away from half-filling, the

FIG. 5. Comparison of the second-order IPT (solid line) and IPT* (dashed line) to the QMC solutions (solid dots) for the Holstein model at half-filling with phonon frequency $\Omega = 0.5t^*$, interaction strength $g = 0.625t^*$, and temperature $T = t^*/6$. This example is generic for the strong-coupling limit. The self-energy renormalization function (a) and the irreducible vertex function in the CDW channel (b) are pictured. Note that in the strong-coupling regime the QMC vertex becomes quite attractive at low-frequency transfer.
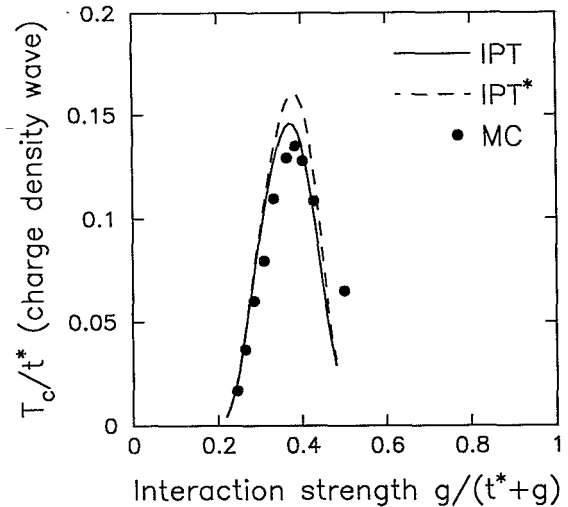
FIG. 6. Transition temperature to the CDW-ordered state at half-filling in the Holstein model at an intermediate phonon frequency ($\Omega = 0.5t^*$). The IPT approximation (solid line) is compared to the IPT* approximation (dashed line) and the QMC results (solid dots). Both approximations are similar to each other and are accurate at predicting the peak height and position. This occurs because the underestimation of the self-energy is canceling the underestimation of the vertex in the calculation of T_c.

CDW instability remains locked at the commensurate point ($X = -1$) until it gives way to a SC instability (incommensurate order may appear in a very narrow region of phase space near the CDW-SC phase boundary[8,13] but is neglected here). In Fig. 7, the phase diagram of the Holstein model is plotted for three values of the interaction strength ($g = 0.4$, $g = 0.5$, and $g = 0.625$). The weak-coupling QMC data[8] ($g = 0.4$) are reproduced most accurately by the perturbative approximations, as expected from the comparison of the self-energy and the vertices in Fig. 3. As the coupling increases to $g = 0.5$ (where the double-well structure begins to form in the effective phonon potential[8]), the approximations become less accurate. The anomalous behavior of the CDW transition temperature not being a maximum at half-filling already appears for the IPT approximation, but the IPT approximation is more accurate at determining the CDW-SC phase boundary. This anomalous behavior in the CDW transition temperature most likely occurs because the approximation is not a conserving approximation. Note that the SC transition temperatures are still accurately reproduced in this regime.

When one is well into the strong-coupling regime ($g = 0.625$) both the IPT and IPT* approximations have large anomalous behavior near half-filling. The CDW-SC phase boundary is also poorly approximated. Clearly both approximations are failing at this large value of the coupling.

Both the IPT and IPT* approximations yield virtually identical results for the Holstein model at a moderate phonon frequency. The self-energy and the irreducible

FIG. 7. Phase diagram of the Holstein model with $\Omega = 0.5t^*$ at three different coupling strengths ($g = 0.4, 0.5, 0.625$). The solid dots are the QMC solutions with CDW order, and the open triangles are the QMC results with SC order (the dotted lines are a guide to the eye). The kinks in the solid (IPT) and dashed (IPT*) lines occur at the CDW-SC phase boundaries. Note the anomalous behavior of the CDW transition temperature not being maximal at half-filling sets into the approximate theories as the coupling strength increases.

vertex functions are poorly reproduced, implying that third-order diagrams are important when the interaction is retarded, but remarkably, the transition temperatures are reproduced quite well. At half-filling both approximations show a peak in the CDW transition temperature. Off of half-filling, the SC transition temperature is determined more accurately than the CDW transition temperature (indeed anomalous behavior enters into the CDW channel near half-filling when the interaction strength is large enough). The phase boundary between CDW and SC order is also accurately reproduced.

IV. HUBBARD MODEL

The Hubbard model in Eq. (3) is the infinite phonon frequency limit ($\Omega \to \infty$) of the Holstein model. The Hubbard model has an electron-electron interaction that only occurs between electrons with opposite spins. This happens because of the cancellation of the direct and exchange diagrams which causes all electron-electron interactions between like-spin particles to vanish. The perturbation theory becomes much simpler in the Hubbard model case, because of this reduction of diagrams, and can be performed to higher order. Here the truncated IPT approximation will be carried out to fourth order, and will be compared to the QMC simulations[3] to determine their accuracy. Previous work has concentrated on second-order conserving approximations,[11,12] third- and fourth-order conserving approximations,[14] or the fluctuation-exchange (FLEX) approximation.[11,14]

One expects that a truncated approximation will be superior to an infinite summation of random-phase approximation (RPA) bubbles and particle-hole and particle-particle ladders because the many-body problem reduces to a self-consistently embedded Anderson impurity model, and the analysis of Yosida and Yamada[18] has shown that the total fourth-order corrections to the self-energy are an order of magnitude smaller and opposite in sign to the fourth-order contribution of the FLEX approximation. The irreducible vertex functions should have similar effects, but have not yet been analyzed in detail.

The diagrammatic expansion for self-energy (in the IPT approximation) of the Hubbard model is given in Fig. 8. Here, the solid lines denote the bare Green's function G_0 and the dotted lines denote the instantaneous Coulomb interaction U. The first line includes the first-order Hartree contribution (which is a constant that is absorbed into a renormalized chemical potential), the second-order contribution, and the third-order particle-hole and particle-particle ladders. The second line contains the fourth order contributions from the RPA bubbles and the particle-hole and particle-particle ladders. The third and fourth lines include all of the remaining diagrams that enter at fourth order. The fifth line contains the insertion of the second-order self-energy into the second-order diagrams. The irreducible vertex functions are too cumbersome to represent diagrammatically. Explicit formulas for the electronic self-energy of the Hubbard model through fourth order and for the
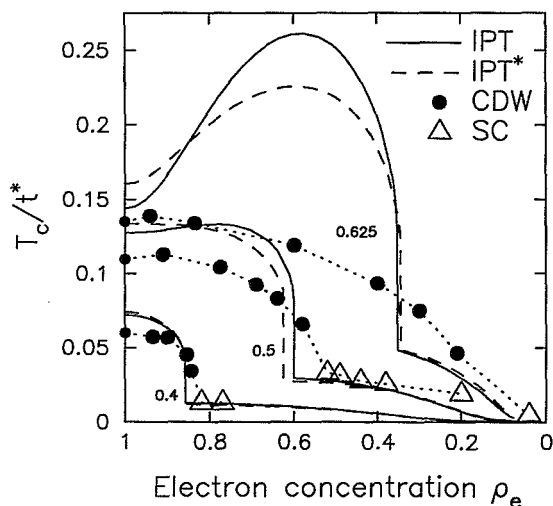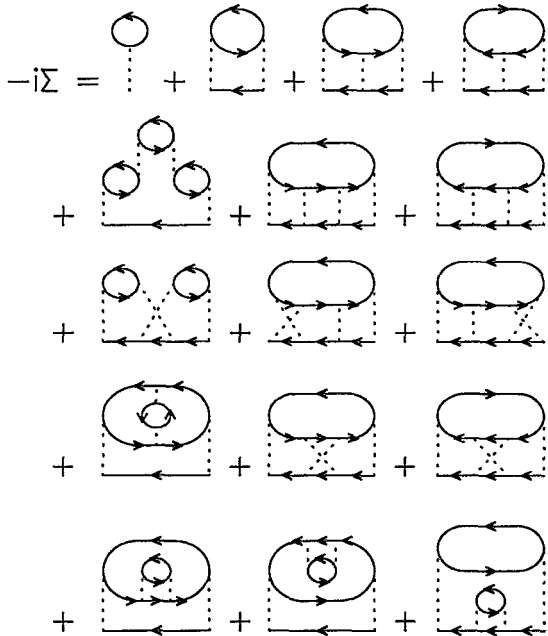
FIG. 8. Self energy diagrams for the Hubbard model through fourth order. The solid lines denote the *bare* electronic Green's functions, and the dotted lines are the Coulomb interaction. The first two lines contain all of the bubbles and ladders through fourth order. The middle two lines are the remaining diagrams that enter first at fourth order. The last line includes the second-order self-energy insertions into the second-order diagrams. At half-filling the odd-order contributions to Σ vanish, and each of the three fourth-order contributions on the same line yield the same contribution to Σ.

CDW vertex have been given before[14] (except for the second-order self-energy insertions into the second-order diagrams which are easily determined). Once again IPT denotes the approximation where the irreducible vertex is strictly truncated at a given order, while the IPT* approximation determines the vertex functions by using the dressed Green's functions.

Since the Hubbard-model interaction is particle-hole symmetric, the half-filled band corresponds to $\mu = 0$, and the Green's functions are purely imaginary. The odd-order contributions to the self-energy all vanish and each of the fourth-order contributions on a given line in Fig. 8 are identical.[18] Since the self-energy is an even function of U at half-filling, but the irreducible vertex function contains both even and odd powers of U, the only difference between a truncated approximation of order $2n$ and of order $2n+1$ is that the irreducible vertex function is larger for the odd-order approximation. Therefore, we expect that an even-order approximation will underestimate the transition temperature (in weak coupling) and an odd-order approximation will overestimate T_c.

One of the most remarkable results of Yosida and Yamada is that the total fourth-order contribution to the self-energy is an order of magnitude smaller than any of its component pieces. One can ask if the same near cancellation holds in the mapping to the infinite-dimensional

lattice. The answer is affirmative, as can be seen in Fig. 9, where each of the individual contributions to the self-energy are plotted at half-filling for $U = -1$ and $T = 0.05$. The dashed line shows the second-order contribution to the self-energy. The dotted lines are each of the four different fourth-order contributions. FLEX denotes the first fourth-order contribution corresponding to the fourth-order bubbles and ladders. Line 2 and line 3 denote the contributions arising from the next two lines respectively in Fig. 8, and IPT is used to denote the contributions arising from the second-order self-energy insertions into the second-order diagram (the last line of Fig. 8). The total of all of the fourth-order diagrams is plotted with the solid line. One can see that the remarkable near cancellation of the fourth-order diagrams still holds in infinite dimensions, and in this case the fourth-order contribution is the same sign, but more than an order of magnitude smaller than the FLEX contribution at fourth order.

A comparison of the different approximation schemes versus the exact QMC results is given in Figs. 10–12 for three different values of U. The second-order and third-order approximations employ an energy cutoff of 256 positive Matsubara frequencies; the fourth-order approximation uses 64 positive Matsubara frequencies. In Fig. 10(a) the self-energy renormalization function is plotted for the
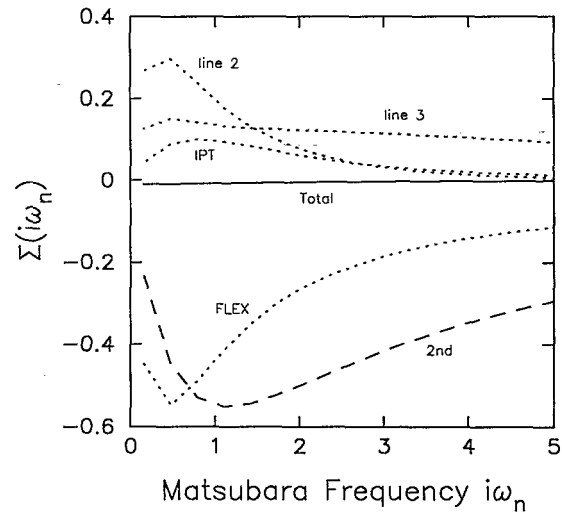

FIG. 9. Near cancellation of the fourth-order contributions to the self-energy. The second-order contribution to the self-energy (dashed line) is compared to each of the four fourth-order contributions (dotted lines) and the net fourth-order contribution (solid line) at $U = -t^*$, $T = t^*/20$, and half-filling. The dotted line denoted FLEX corresponds to the first line of the fourth-order contributions in Fig. 8. The labels line 2 and line 3 denote the next two lines of fourth-order contributions in Fig. 8, and the label IPT refers to the last line in Fig. 8 corresponding to the second-order self-energy insertions into the second-order diagrams. Note that the total contribution of the fourth-order diagrams is an order of magnitude smaller than any of the individual classes of diagrams in Fig. 8, and that it is the same sign as the FLEX contributions.

two different approximations at $U = -1$ ($T = 0.05$). Note that the fourth-order approximation virtually reproduces the QMC results. In Fig. 10(b) the even components of one row of the irreducible vertex function for the CDW channel are compared for $U = -1$ in the IPT approximation. All of the approximations are in reasonable agreement with the QMC results, but the accuracy is significantly reduced relative to what was found for the self-energy. The IPT* approximation is compared to the QMC results in Fig. 10(c). These results are similar to the IPT approximation, but perhaps not as accurate.

As the coupling strength is increased to $U = -2$ ($T = 0.125$) the self-energy is becoming bracketed by the two

low-order approximations, with the fourth-order approximation overestimating the self-energy, and the second-order approximation underestimating the self-energy, as shown in Fig. 11(a). The CDW vertex is plotted in Fig. 11(b) for the IPT approximation. One can see strong-coupling effects beginning to enter as the QMC vertex becomes more attractive at low-frequency transfer than predicted by the even-order approximations. The third-order IPT approximation is producing the correct qualitative shape of the vertex, but it is overestimating the magnitude by a large amount. The IPT* approximation is shown in Fig. 11(c). Here the two different methods for calculating the vertex yield quite different
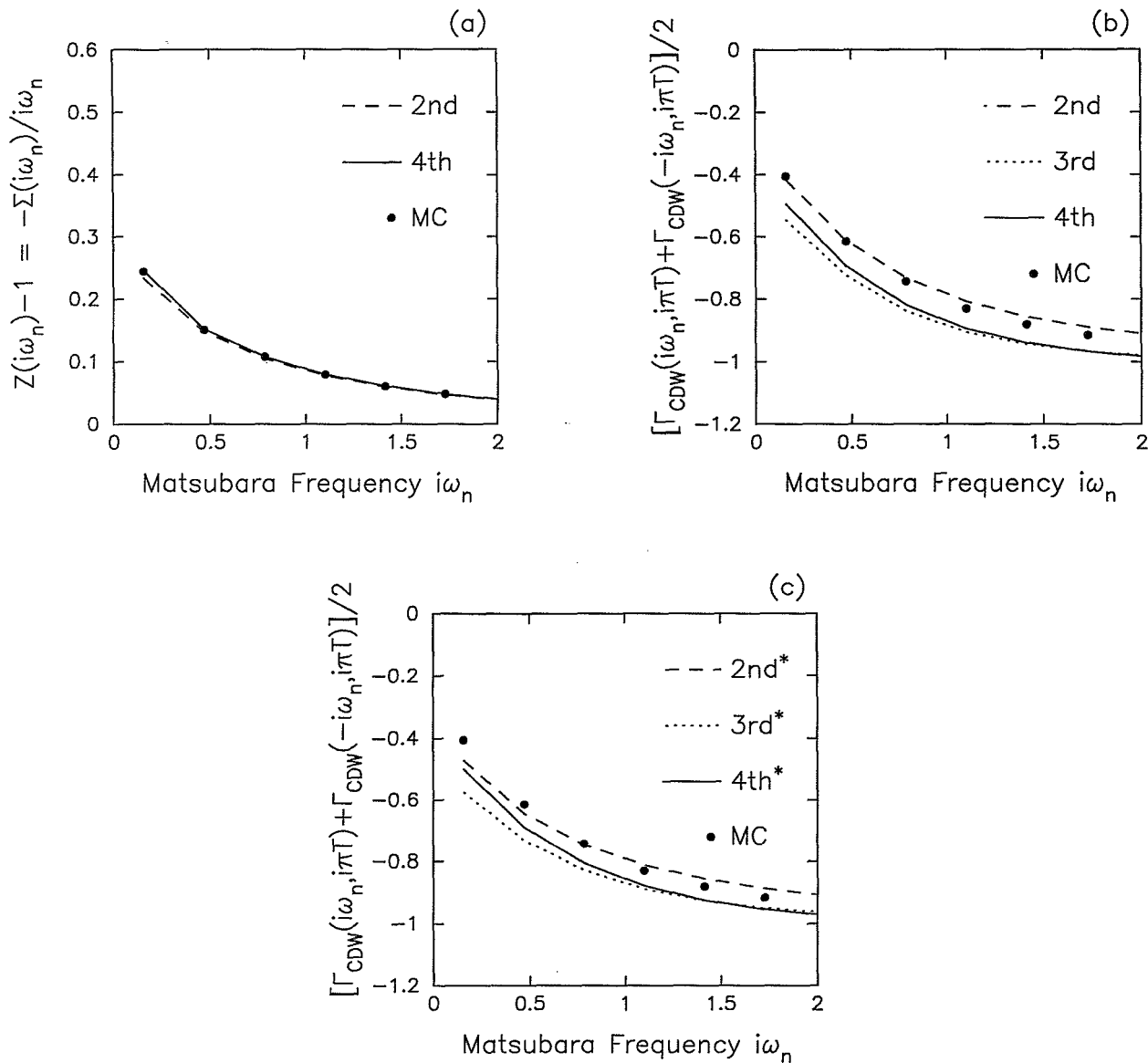

FIG. 10. Comparison of the IPT and IPT* approximations to the QMC solutions for the Hubbard model at half-filling in the limit of weak coupling ($U = -t^*, T = t^*/20$). The second-order (dashed line), third-order (dotted line), and fourth-order (solid line) approximations are compared to the QMC solutions (solid dots). In (a) the self-energy renormalization function is plotted against Matsubara frequency. In (b) the even component of the first column of the irreducible vertex function in the CDW channel is plotted in the IPT approximation, and in (c) it is plotted in the IPT* approximation.

results. In the IPT* approximation, all orders are showing a weakening of the vertex at lower frequencies, which is not present in the QMC data.

Finally, at a rather strong value of the coupling ($U = -3$, $T = 0.167$), where the transition temperature reaches its maximal value, the self-energy is still reproduced quite accurately by both orders of the IPT [see Fig. 12(a)]. The vertices are, however, quite poorly approximated. In Figs. 12(b) and 12(c) the results for the IPT and IPT*, respectively, are presented. The QMC vertex is becoming strongly attractive here. Only the third-order IPT approximation has the correct qualitative behavior, but it overestimates the magnitude of the vertex. The IPT* approximation produces a fairly flat frequency dependence to the vertex which is quite accu-

rate at all but the lowest-frequency transfers (where it is almost an order of magnitude too small).

The conclusion that we can draw from this comparison of the self-energy and irreducible vertex functions is that the IPT approximation is quite accurate for the self-energy, but is a rather poor approximation for the irreducible vertex function. It is known that the reason why the IPT is so accurate for the self-energy arises from the fact that it properly reproduces the atomic limit,[21,4] but it is possible that it does not produce the atomic limit for the irreducible vertex functions. If this were the case, one could try another *ad hoc* interpolation scheme that interpolates between the perturbative result for the vertex, and the atomic limit, to provide a more accurate approximation.
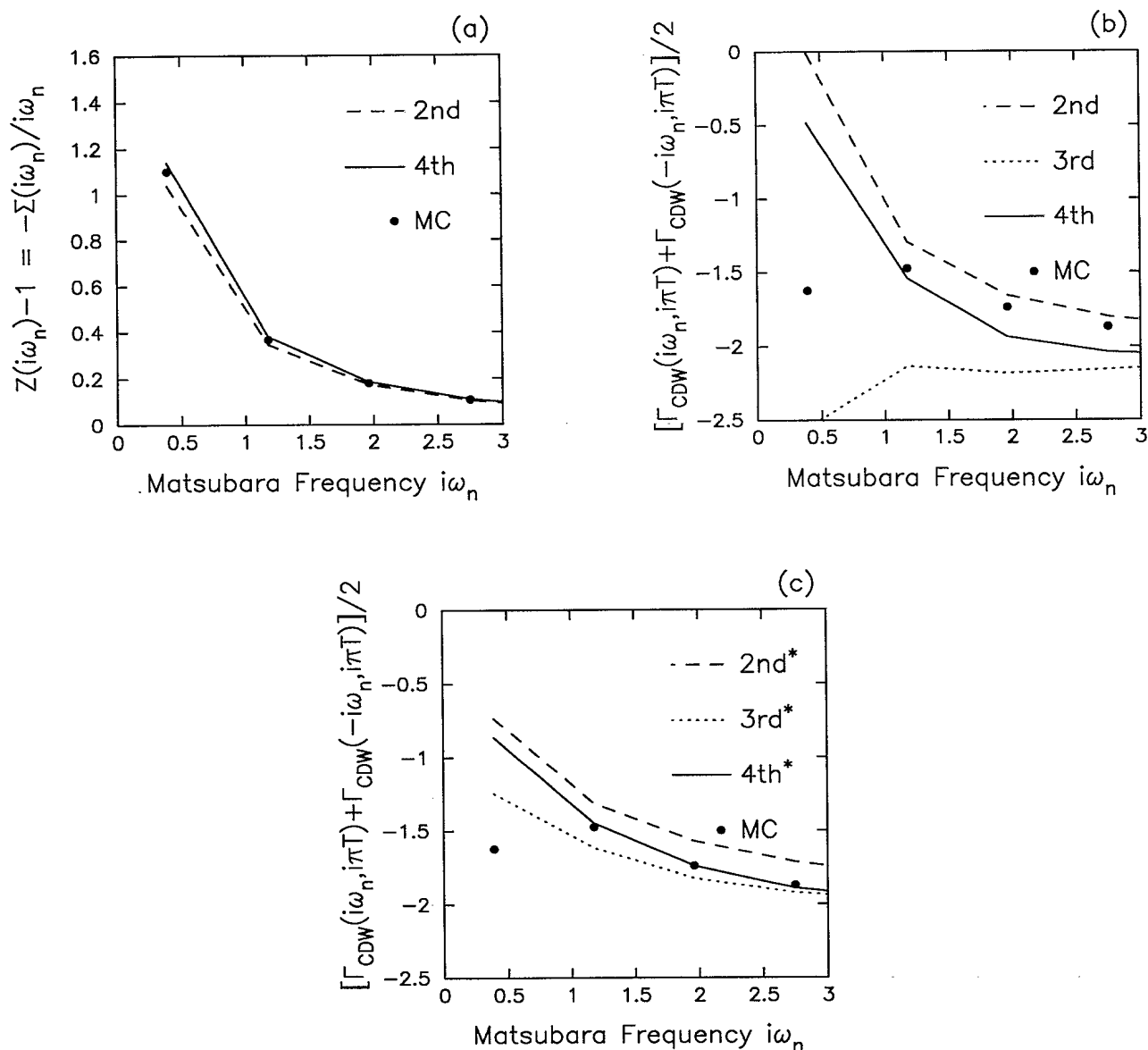

FIG. 11. Same as in Fig. 10, but with a stronger value of the coupling ($U = -2t^*, T = t^*/8$). The self-energy is still reproduced accurately by all orders, but only the third-order IPT approximation has the correct qualitative behavior for the vertex.

Note also that since the self-energy is reproduced quite accurately by the IPT, but the magnitude of the vertex is grossly underestimated, the transition temperature will drop too rapidly in the strong-coupling regime (with the exception of the third-order IPT approximation where the transition temperature will grow too rapidly). This is illustrated by plotting the transition temperature for the CDW transition at half-filling in the attractive Hubbard model as a function of U (Fig. 13) and comparing to the QMC solution.[3] In the IPT approximation [Fig. 13(a)], the peak in T_c as a function of U is properly reproduced for the even-order approximations, but not for the odd-order one. The transition temperature decreases too rapidly in the strong-coupling regime because of the underestimation of the vertex. In the IPT*

approximation [Fig. 13(b)], all orders have a peak in T_c as a function of U. The third-order approximation is the most accurate here, because it has the most attractive vertex, but even in this case the quantitative agreement with the QMC is not as good as was found for the truncated conserving approximations,[14] where the transition temperature did not have a peak, but the underestimation of the self-energy compensated for the underestimation of the vertex to produce reasonably accurate transition temperatures into the strong-coupling regime.

The doping dependence of the SC transition temperature is plotted in Fig. 14 for both the second- and third-order IPT and IPT* approximations and $U = -1$. Even at this weak a value of the coupling strength, the second-order IPT and IPT* approximations show the anomalous
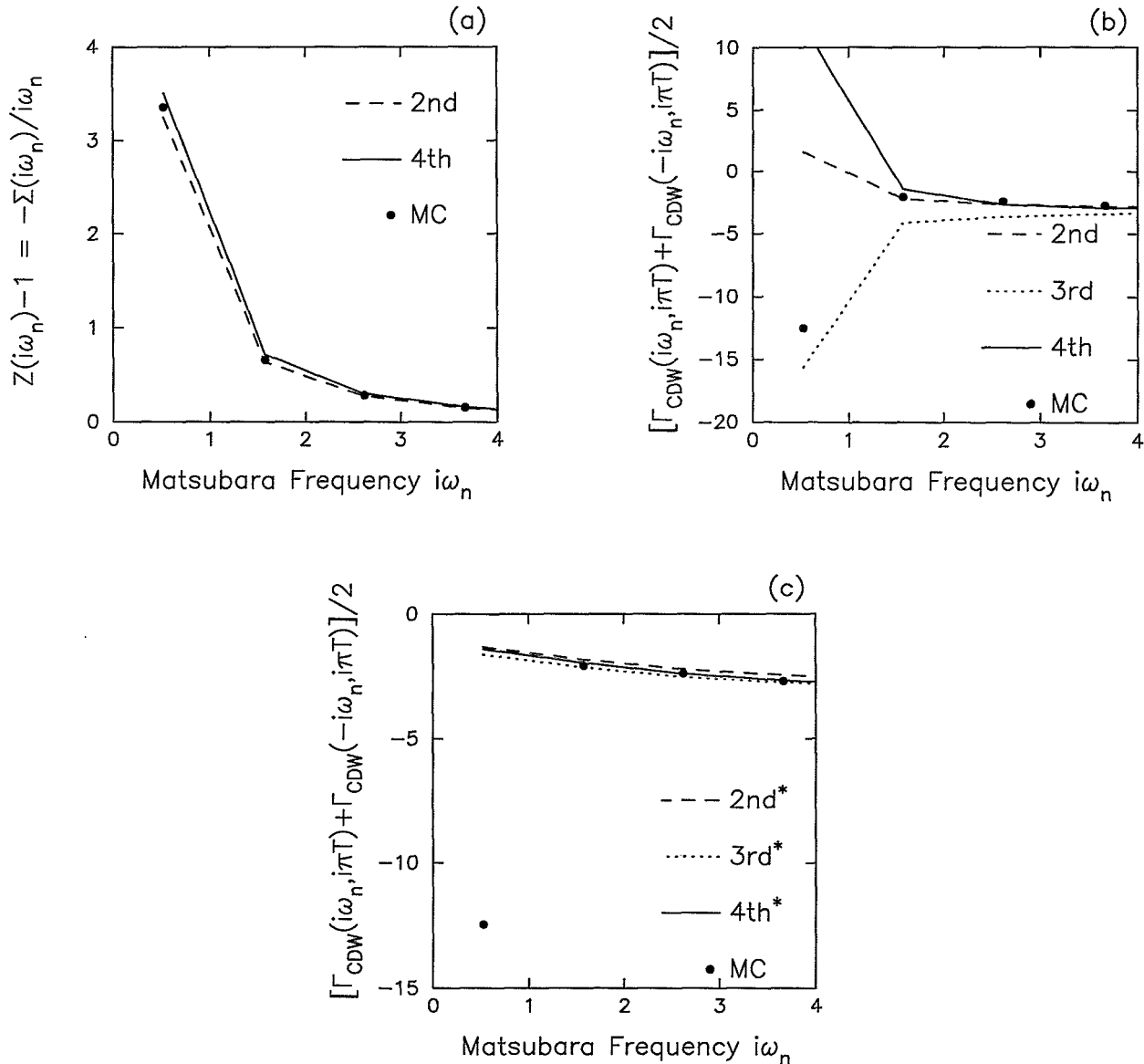

FIG. 12. Same as in Fig. 10, but with a stronger value of the coupling ($U = -3t^*, T = t^*/6$). The self-energy is still reproduced accurately by all orders, but only the third-order IPT approximation has the correct qualitative behavior for the vertex.

behavior of an increase in T_c for small dopings off of half-filling. A third-order approximation works much better (because third-order contributions to the self-energy enter when the electron concentration is not equal to 1), and does not display the anomalous behavior (at this value of U). Once again, the IPT* approximation is more robust against the anomaly in T_c, but all IPT approximations quickly fail as the coupling strength increases beyond $U = -1$ (because they fail at half-filling as shown in Fig. 13).

FIG. 14. Transition temperature to the SC state in the Hubbard model as a function of electron concentration at $U = -1$. The second-order IPT (solid line), third-order IPT (dotted line), second-order IPT* (dashed line), and third-order IPT* (chain-dotted line) are compared to the QMC results (open triangle). Note that both second-order approximations display anomalous behavior near half-filling even for this small a value of the interaction strength.
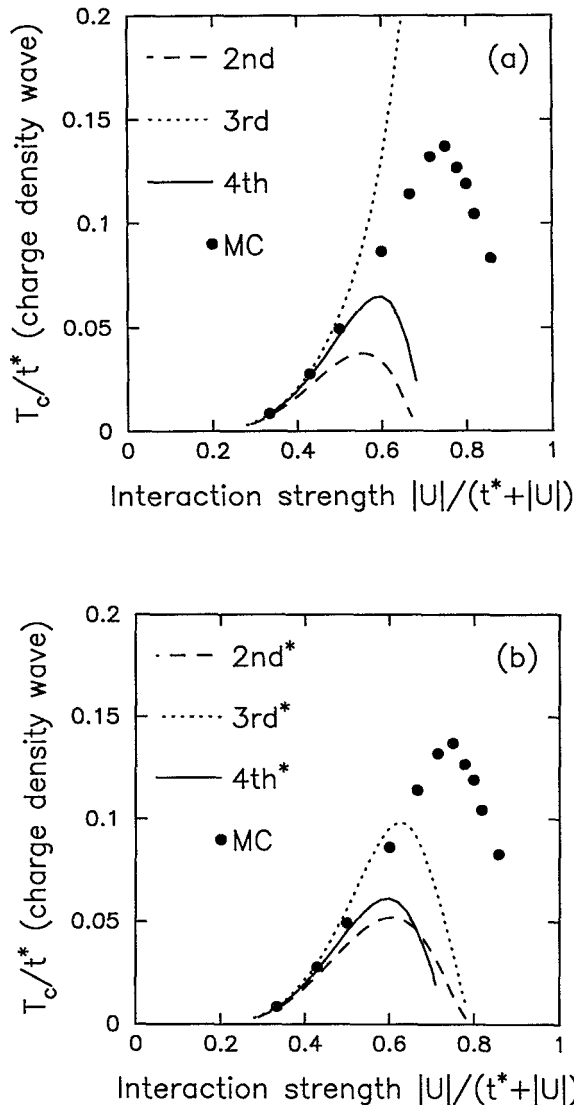

FIG. 13. Transition temperature to the CDW-ordered (and SC-ordered) state in the Hubbard model at half-filling. The second-order (solid line), third-order (dotted line), and fourth-order (solid line) IPT (a) and IPT* (b) approximations are compared to the QMC results (solid dots). Note that the transition temperature curves all have a turnover (except for the third-order IPT approximation) because the vertex is underestimated as the coupling strength increases. The third-order IPT approximation does not turn over because the vertex is overestimated.
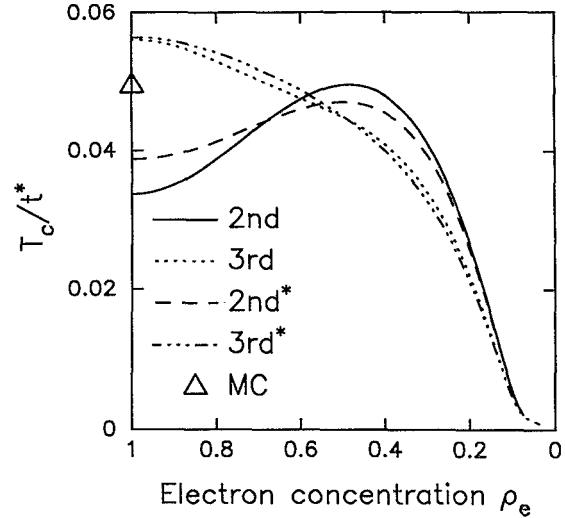
V. CONCLUSIONS

The iterated perturbation theory approximation[17] has been applied to the attractive Holstein and Hubbard models in infinite dimensions. This weak-coupling theory is not a conserving approximation because it corresponds to a strictly truncated perturbation series for the self-energy. The vertex functions are either approximated with a strictly truncated perturbation series too (IPT), or with a truncated perturbation series that includes all self-energy insertions (IPT*).

At half-filling, these approximate theories are accurate in reproducing the electronic self-energy (for the Holstein model, the accuracy increases as the phonon frequency increases) but do not reproduce the correct behavior of the irreducible vertex functions in the strong-coupling regime.

In particular, for the half-filled Hubbard model, the IPT is a very accurate approximation for the self-energy of the Hubbard model, but is a poor approximation for the irreducible vertex functions a low-frequency transfer. As a result, the transition temperature does in general display a peak (because of the large self-energy renormalizations), but decreases too rapidly in the strong-coupling regime.

The IPT is a much less accurate approximation for the self-energy of the Holstein model at finite phonon frequency (indicating the importance of higher-order diagrams). The IPT is also a poor approximation for the vertex functions, but, remarkably, the transition temperatures are quite accurately approximated both at half-filling and off of half-filling (for small enough coupling

strength). The peak position and height of T_c at half-filling are reproduced well, as is the doping dependence of T_c up to the region of parameter space where a double-well structure begins to develop in the effective phonon potential.

As both of these systems are doped away from half-filling, the transition temperatures (to either a CDW or a SC) display the anomalous behavior of initially *increasing* with doping. This anomalous behavior first enters at some critical value of the coupling, and becomes worse as the coupling strength is increased. For the Holstein model (with $\Omega = 0.5$) this critical coupling lies near $g \approx 0.5$, whereas for the Hubbard model it occurs at $|U| \approx 1$. Third-order diagrams tend to push this anomaly out to larger values of interaction strength as expected because the third-order contributions to the self-energy can be large as the system is doped off of half-filling.

As a final summary, the IPT is a highly accurate approximation for the self-energy when the interaction is instantaneous, but generally underestimates the magnitude of the vertex functions at low-frequency transfer; it does not approximate the transition temperature well in the strong-coupling regime. The IPT is a less accurate approximation for both the self-energy and vertices for retarded interactions, but is much more accurate in determining transition temperatures because the errors in the self-energy and the vertices tend to cancel in the

determination of T_c. The the explanation for this behavior is that the IPT is an accurate approximation when third-order terms can be neglected. This occurs for the self-energy of the Hubbard model at half-filling, but is not true for the self-energy when the interaction is retarded or the filling is different from 1, or for the irreducible vertex functions. Qualitatively the IPT approximation is better than the same order conserving approximation[14] for the self-energy of the Hubbard model, but the transition temperatures are better approximated (quantitatively) by the conserving approximation. For the Holstein model, the IPT is superior to the conserving approximation in all aspects except for the anomalous behavior in T_c near half-filling and for large enough coupling strength.

ACKNOWLEDGMENTS

[1] W. Metzner and D. Vollhardt, Phys. Rev. Lett. **62**, 324 (1989).

[2] J. E. Hirsch and R. M. Fye, Phys. Rev. Lett. **56**, 2521 (1986).

[3] M. Jarrell, Phys. Rev. Lett. **69**, 168 (1992); M. Jarrell and Th. Pruschke, Z. Phys. B **90**, 187 (1993); Th. Pruschke, D. L. Cox, and M. Jarrell, Phys. Rev. B **47**, 3553 (1993).

[4] M. J. Rozenberg, X. Y. Zhang, and G. Kotliar, Phys. Rev. Lett. **69**, 1236 (1992).

[5] A. Georges and W. Krauth, Phys. Rev. Lett. **69**, 1240 (1992); Phys. Rev. B **48**, 7167 (1993).

[6] V. Janiš, M. Ulmke, and D. Vollhardt, Europhys. Lett. **24**, 287 (1993).

[7] M. Jarrell, H. Akhlaghpour, and Th. Pruschke, Phys. Rev. Lett. **70**, 1670 (1993).

[8] J. K. Freericks, M. Jarrell, and D. J. Scalapino, Phys. Rev. B **48**, 6302 (1993); Europhys. Lett. **25**, 37 (1994); J. K. Freericks and M. Jarrell, in *Computer Simulations in Condensed Matter Physics*, edited by D. P. Landau, K. K. Mon, and H.-B. Schüttler (Springer-Verlag, Heidelberg, 1994), Vol. VII.

[9] J. K. Freericks, Phys. Rev. B **48**, 3881 (1993).

[10] V. Janiš and D. Vollhardt, Int. J. Mod. Phys. B **6**, 731 (1992); Z. Phys. B. **91**, 317 (1993); V. Janiš, J. Mašek, and D. Vollhardt, *ibid.* **91**, 325 (1993); Y. M. Li and N. d'Ambrumenil, Mod. Phys. Lett. B **6**, 1827 (1992); Phys. Rev. B **49**, 6058 (1994).

[11] E. Müller-Hartmann, Z. Phys. B **74**, 507 (1989); **76**, 211 (1989); B. Menge and E. Müller-Hartmann, *ibid.* **82**, 237 (1991).

[12] D. S. Hirashima, Phys. Rev. B **47**, 15428 (1993).

[13] S. Ciuchi, F. de Pasquale, C. Masciovecchio, and D. Feinberg, Europhys. Lett. **24**, 575 (1993).

[14] J. K. Freericks and D. J. Scalapino, Phys. Rev. B **49**, (1994); J. K. Freericks, *ibid.* **50**, 403 (1994).

[15] G. Baym and L. P. Kadanoff, Phys. Rev. **124**, 287 (1961); G. Baym, *ibid.* **127**, 1391 (1962); N. E. Bickers and D. J. Scalapino, Ann. Phys. (N.Y.) **193**, 206 (1989).

[16] J. A. White, Phys. Rev. B **45**, 1100 (1992).

[17] A. Georges and G. Kotliar, Phys. Rev. B **45**, 6479 (1992).

[18] K. Yosida and K. Yamada, Prog. Theor. Phys. **46**, 244 (1970); K. Yamada, *ibid.* **53**, 970 (1975); K. Yosida and K. Yamada, *ibid.* **53**, 1286 (1975); K. Yamada, *ibid.* **54**, 316 (1975); **55**, 1345 (1976); **62**, 354 (1979).

[19] V. Zlatić and B. Horvatić, Phys. Rev. B **28**, 6904 (1983).

[20] B. Horvatić and V. Zlatić, Phys. Status Solidi B **99**, 251 (1980); **111**, 65 (1982); Phys. Rev. B **30**, 6717 (1984); Solid State Commun. **54**, 957 (1985); V. Zlatić, B. Horvatić, and D. Šokčević, Z. Phys. B **59**, 151 (1985); B. Horvatić, D. Šokčević, and V. Zlatić, Phys. Rev. B **36**, 675 (1987).

[21] J. Ferrer, A. Martín-Rodero, and F. Flores, Phys. Rev. B **36**, 6149 (1987).

[22] H. L. Neal, Phys. Rev. B **32**, 5002 (1985); Phys. Rev. Lett. **66**, 818 (1991); H. L. Neal and D. J. Collins, Phys. Rev. B **48**, 4299 (1993).

[23] *Superconductivity*, edited by R. Parks (Marcel Dekker, Inc., New York, 1969).

[24] P. B. Allen and R. C. Dynes, Phys. Rev. B **12**, 905 (1975); P. B. Allen and B. Mitrović, Solid State Phys. **37**, 1 (1982); J. P. Carbotte, Rev. Mod. Phys. **62**, 1027 (1990); H.-S. Wu, Z.-Y Weng, G. Ji, and Z.-F. Zhou, J. Phys. Chem. Solids **48**, 395 (1987).

[25] A. B. Migdal, Zh. Eksp. Teor. Fiz. **34**, 1438 (1958) [Sov. Phys. JETP **7**, 999 (1958)].

[26] G. M. Eliashberg, Zh. Eksp. Teor. Fiz. **38**, 966 (1960) [Sov. Phys. JETP **11**, 696 (1960)].

[27] T. Holstein, Ann. Phys. (N.Y.) **8**, 325 (1959).

[28] J. Hubbard, Proc. R. Soc. London A **276**, 238 (1963).

[29] H. Schweitzer and G. Czycholl, Z. Phys. B **77**, 327 (1990).

[30] W. Metzner, Phys. Rev. B **43**, 8549 (1991).

[31] U. Brandt and C. Mielsch, Z. Phys. B **75**, 365 (1989).

[32] F. J. Ohkawa, Phys. Rev. B **44**, 6812 (1991); Prog. Theor. Phys. Suppl. **106**, 95 (1991).

[33] R. M. Noack, D. J. Scalapino, and R. T. Scalettar, Phys. Rev. Lett. **66**, 778 (1991).

[34] V. Zlatić and B. Horvatić, Solid State Commun. **75**, 263 (1990).

[35] C. S. Owen and D. J. Scalapino, Physica **55**, 691 (1971).

[36] P. G. J. van Dongen, Phys. Rev. Lett. **67**, 757 (1991).

[37] A. Martín-Rodero and F. Flores, Phys. Rev. B **45**, 13008 (1992).